AJBAR Vol. 3(1), February 2024: 65-87, ISSN: 2811-2881

Arid Zone Journal of Basic and Applied Research

Faculty of Science, Borno State University Maiduguri, Nigeria

Journal homepage: https://www.azjournalbar.com

Research Article

Application of Static Synchronous Compensator for Improvement of Power System Transient Stability

Olaogun P. O.[1], Adebisi O. I.[1], Adejumobi I. A.[1] and Adams D. O.[2]

[1]Department of Electrical and Electronics Engineering, Federal University of Agriculture, Abeokuta, Ogun State, Nigeria

[2]Department of Mathematics, Federal University of Agriculture, Abeokuta, Ogun State, Nigeria

*Corresponding author's Email: olayemiolaogunpeter@gmail.com, doi.org/10.55639/607.454443

ARTICLE INFO:

Keywords:
Modified Euler,
Newton- Rapson,
Power flow,
STATCOM,
Transient stability

ABSTRACT

Transient stability is the power system's ability to maintain synchronism when exposed to severe disturbances such as loss of generation, rapid load changes, transmission lines tripping, switching operations and faults. Transient instability causes cascading outages, system collapse and economical losses. This study employed static synchronous compensator (STATCOM) for power system transient stability improvement. The system's steady state and transient responses were respectively modelled with Newton-Raphson power flow and modified-Euler linearized swing equations. A balanced three-phased short circuit fault was introduced on selected buses for transient stability analysis. The steady state and transient responses of the system were simulated with and without STATCOM. The critical fault clearing time (CFCT) was obtained from the generators' swing curves. The IEEE 9-bus and 14-bus power networks were used as test cases. The voltage magnitudes of all buses in both networks fell within the specified 0.95 to 1.1 p.u. voltage limit with and without compensation. The total active line loss on IEEE 9-bus and 14-bus networks which were 4.641 and 13.514 MW without compensation reduced to 4.600 and 13.014 MW, respectively with STATCOM's application. The total reactive line losses of both networks which were 92.160 and 31.393 MVAr without compensation decreased to 90.160 and 30.693 MVAr, respectively with STATCOM' utilization. The CFCT for fault on bus 8 of the IEEE 9-bus system without compensation were 0.2100 and 0.2700 s for generators 2 and 3, respectively. The system's stability was, however, extended beyond 0.2700 s due to compensation from STATCOM. In the case of IEEE 14-bus system, the CFCT for fault on bus 6 was 0.36364 s for generators 2, 3, 4 and 5, respectively without compensation. The STATCOM inclusion, however, enhanced the system's stability beyond 0.36366 s where all the four had lost synchronism. This work established that the use of STATCOM on the considered networks appropriately extended the CFCT such that the stability of the systems was not lost in the event of fault application via robust compensation of reactive power.

Corresponding author: Olaogun P. O, **Email:** olayemiolaogunpeter@gmail.com
Department of Electrical and Electronics Engineering, Federal University of Agriculture, Abeokuta, Ogun State, Nigeria

INTRODUCTION

An electric power grid usually is not a fail-free system. Due to its complexity, the system is susceptible to severe disturbances such as short circuit faults, rapid changing of loads, tripping of transmission lines and loss of generation during operation, leading to transient stability problem (Fan *et al.*, 2016; Naveed *et al.*, 2019; Noaman *et al.*, 2017). Transient stability, by definition, is the ability of a power system to maintain synchronism after been subjected to major disturbances (Alhamrouni *et al*., 2020).

Conventional methods such as mechanical switches, creation of more generation plants and transmission lines, capacitor banks among others had been adopted in the past for transient stability improvement in electricity grids. However, these techniques are slow in action with high cost of maintenance and possible wear and tear of the mechanical parts. This, therefore, paves the way for the use of flexible alternating current transmission systems (FACTS) devices (Radmehr *et al*., 2017). FACTS gain its acceptability because it can improve transmission system operation and control, reduce investment cost, increase system security and reliability, increase power transfer capabilities and enhance the quality of electrical energy delivered to end-users (Adebisi *et al*., 2018; Asare *et al*., 1994; Jokojeje *et al*., 2015a; Jokojeje *et al*., 2015b).

A survey of literature has shown that the FACTS family comprises various members including interline power flow controller (IPFC), static synchronous series compensator (SSSC), static var compensator (SVC), thyristor controlled series capacitor (TCSC) and unified power flow controller (UPFC) with unique qualities that adapt them suitably to the applications in which they are employed (Fadadu & Lotiya 2016; Garg & Khan 2020; Gupta & Pahariya 2017; Mbae & Nwulu 2022; Praveen et al 2016; Sharan *et al.*, 2019). On this account, several investigations have been conducted on the potentials of these controllers for power system transient stability enhancement with some promising outcomes (Barua *et al.*, 2021; Fathollahi *et al.*, 2022; Ghaedi *et al.*, 2021; Gurijala *et al.*, 2021; Singh & Singh, 2022; Shrivastava *et al.*, 2021). However, since of occurrence of severe disturbances in power systems is unpredictable and unavoidable considering the complicated structure of the networks, there is, therefore, the need for more and continuous investigations in the area of power system transient stability analysis and improvement to curtail the disastrous effects of the major disturbances such as voltage collapse, cascading failures and equipment damage.

For the purpose of this work, STATCOM was considered for transient stability improvement because it offers a better level of utilization of the existing facilities in the power system network taking into account its flexibility, cost-effectively, quick response and high reactive power compensation capability (Narayana & Gudapati 2021; Sawkmie *et al*., 2018). When under- or over-voltage condition develops in the system, STATCOM has the potential to quickly increase or decrease the voltage via reactive power injection or absorption and therefore, regulates the voltage at the connection point to prevent instability from occurring in the system. According to Liu *et al.* (2017) and Sharan *et al.* (2019), this action enables it to operate in two possible modes - under-excited or over-excited states. In the under-excited state, STATCOM draws reactive power from power networks, while it injects same into the systems in the over-excited state. Hence, its ability to resolve voltage-related issues. Integration of FACTS device such as STATCOM in power system networks will have a great effect in enhancing the performance of the systems including transient instability control.

METHODOLOGY

The Load Flow Formulation

Load flow in Power system is very crucial because it is a key tool for design and analysis of

power systems in the areas of planning and operation, power transfer between utilities, economic scheduling, contingency and transient stability studies (Glover & Sarma, 2002; Gupta, 2011; Hadi, 2008; Kothari & Nagrath, 2008).

Load flow in this study was formulated with a typical power system bus shown in Figure 1 considered. Application of KCL to the bus system in Figure 1 yields equation (1) and (2):

$$I_i = V_i \sum_{j=0}^{n} y_{ij} - \sum_{j=1}^{n} y_{ij} V_j \qquad j \neq i \tag{1}$$

$$I_i = \sum_{j=1}^{n} Y_{ij} V_j \tag{2}$$

Where I_i, V_i, y_{ij}, Y_{ij} and V_j respectively denote supplied current at bus *i*, voltage at bus *i*, admittance of line *i-j*, element of bus admittance derived from admittance of line *i-j* and voltage of bus *j*.

The use of polar form of Y_{ij} and V_j in equation (2) produced equation (3):

$$I_i = \sum_{j=1}^{n} |Y_{ij}||V_j| \angle \theta_{ij} + \delta_j \tag{3}$$

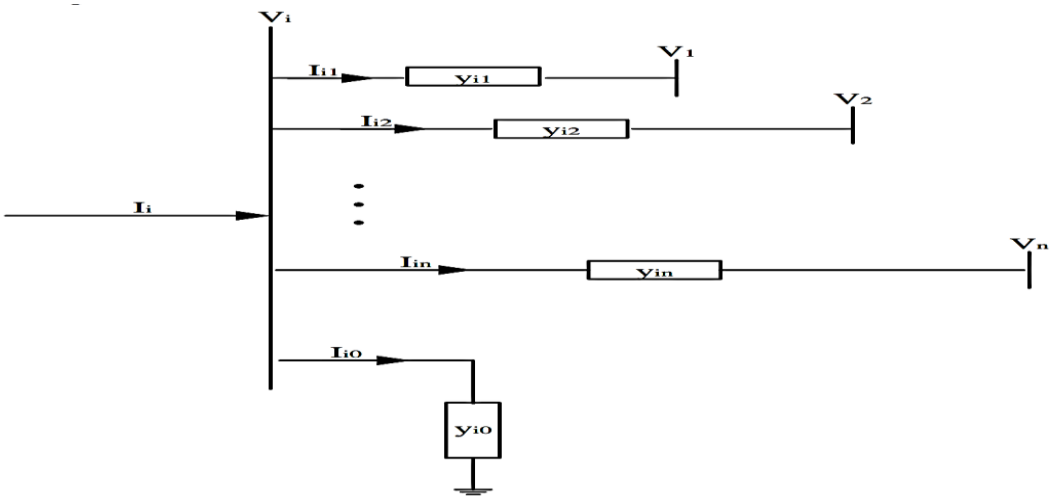

Figure 1: An n-bus structure of power system (Gupta, 2011; Hadi, 2008; Kothari & Nagrath, 2008)

Where $|Y_{ij}|$, $|V_j|$, θ_{ij} and δ_j denote magnitude of admittance of line *i-j*, magnitude of voltage at bus *j*, angle of admittance of line *i-j* and angle of voltage at bus *j*.

The supplied power at bus *i* takes an expression of equation (4):

$$P_i - jQ_i = V_i^* I_i \tag{4}$$

Where P_i and Q_i respectively represent bus *i* active and reactive powers.

Substitution of equation (3) into equation (4) and decoupling into real and imaginary components produced equations (5) and (6):

$$P_i = \sum_{j=1}^{n} |V_i||V_j||Y_{ij}| cos(\theta_{ij} + \delta_{ij}) \tag{5}$$

$$Q_i = -\sum_{j=1}^{n} |V_i||V_j||Y_{ij}|sin(\theta_{ij}+\delta_{ij}) \quad (6)$$

With $\delta_{ij} = \delta_j - \delta_i$ (7)

Equations (5) and (6) are the static power flow expressions which govern the steady state response of a power system. They are non-linear equations solved via numerical iterative method. These equations were implemented in this study using Newton-Raphson method because of its faster convergence rate, accuracy, and reliability in comparison to other iterative methods (Glover & Sarma, 2002; Gupta, 2011; Hadi, 2008; Kothari & Nagrath, 2008). The Newton- Raphson based power flow equations arising from the linearization of equations (5) and (6) are expressed by equation (7):

$$\begin{bmatrix}\Delta P \\ \Delta Q\end{bmatrix} = \begin{bmatrix}J_1 & J_2 \\ J_3 & J_4\end{bmatrix}\begin{bmatrix}\Delta\delta \\ \Delta|V|\end{bmatrix} \quad (7)$$

Where J_1, J_2, J_3 and J_4 are the elements of the Jacobin matrix, ΔP, ΔQ, $\Delta\delta$ and $\Delta|V|$ are respectively active power, reactive power, bus voltage angle and bus voltage magnitude mismatches.

ΔP, ΔQ, $\Delta\delta$, $\Delta|V|$, J_1, J_2, J_3 and J_4 are expressed by equations (8) to (15):

$$\Delta P = \begin{bmatrix}\Delta P_2^{(k)} \\ \vdots \\ \Delta P_n^{(k)}\end{bmatrix} \quad (8)$$

$$\Delta Q = \begin{bmatrix}\Delta Q_2^{(k)} \\ \vdots \\ \Delta Q_n^{(k)}\end{bmatrix} \quad (9)$$

$$\Delta\delta = \begin{bmatrix}\Delta\delta_2^{(k)} \\ \vdots \\ \Delta\delta_n^{(k)}\end{bmatrix} \quad (10)$$

$$\Delta|V| = \begin{bmatrix}\Delta\left|V_2^{(k)}\right| \\ \vdots \\ \Delta\left|V_n^{(k)}\right|\end{bmatrix} \quad (11)$$

$$J_1 = \begin{bmatrix}\frac{\partial P_2^{(k)}}{\partial\delta_2} & \cdots & \frac{\partial P_2^{(k)}}{\partial\delta_n} \\ \vdots & \ddots & \vdots \\ \frac{\partial P_n^{(k)}}{\partial\delta_2} & \cdots & \frac{\partial P_n^{(k)}}{\partial\delta_n}\end{bmatrix} \quad (12)$$

$$J_2 = \begin{bmatrix}\frac{\partial P_2^{(k)}}{\partial|V_2|} & \cdots & \frac{\partial P_2^{(k)}}{\partial|V_n|} \\ \vdots & \ddots & \vdots \\ \frac{\partial P_n^{(k)}}{\partial|V_2|} & \cdots & \frac{\partial P_n^{(k)}}{\partial|V_n|}\end{bmatrix} \quad (13)$$

$$J_3 = \begin{bmatrix}\frac{\partial Q_2^{(k)}}{\partial\delta_2} & \cdots & \frac{\partial Q_2^{(k)}}{\partial\delta_n} \\ \vdots & \ddots & \vdots \\ \frac{\partial Q_n^{(k)}}{\partial\delta_2} & \cdots & \frac{\partial Q_n^{(k)}}{\partial\delta_n}\end{bmatrix} \quad (14)$$

$$J_4 = \begin{bmatrix} \frac{\partial Q_2^{(k)}}{\partial |V_2|} & \cdots & \frac{\partial Q_2^{(k)}}{\partial |V_n|} \\ \vdots & \ddots & \vdots \\ \frac{\partial Q_n^{(k)}}{\partial |V_2|} & \cdots & \frac{\partial Q_n^{(k)}}{\partial |V_n|} \end{bmatrix} \quad (15)$$

The active and reactive powers mismatches at k[th] iteration and new estimates of the bus voltage angle and magnitude are expressed respectively by equations (16) and (19):

$$\Delta P_i^{(k)} = P_i^{sch} - P_i^{(k)} \quad (16)$$

$$\Delta Q_i^{(k)} = Q_i^{sch} - Q_i^{(k)} \quad (17)$$

$$\delta_i^{(k+1)} = \delta_i^{(k)} + \Delta\delta_i^{(k)} \quad (18)$$

$$V_i^{(k+1)} = \left|V_i^{(k)}\right| + \Delta\left|V_i^{(k)}\right| \quad (19)$$

The voltage and reactive power constraints imposed at bus *i* are expressed by equations (20) and (21) respectively:

$$V_{imin} \leq V_i \leq V_{imax} \quad (20)$$

$$Q_{imin} \leq Q_i \leq Q_{imax} \quad (21)$$

Where V_{imin}, V_{imax}, Q_{imin} and Q_{imax} respectively denote minimum voltage magnitude, maximum voltage magnitude, minimum reactive power supply and maximum reactive power supply at bus *i*.

Dynamics of Synchronous Machine

In a synchronous machine, the rotor's kinetic energy, KE in joule and synchronous speed, ω_{se} in electrical radian/sec are expressed by equations (22) and (23) respectively (Das 2006; Kothari & Nagrath, 2008):

$$KE = \frac{1}{2} J\omega_s^2 \times 10^{-6}\, Mjoule \quad (22)$$

$$\omega_{se} = (\frac{P}{2})\omega_s \quad (23)$$

Where J, ω_s and P respectively represent moment of inertia of the rotor in kg-m^2, synchronous speed in mechanical radian/sec and number of poles in the machine.

Manipulation of equation (22) and (23) produces equations (24) to (25) which are further derivations for the kinetic energy of the rotor of a synchronous machine:

$$KE = \frac{1}{2}\left[\left(J\left(\frac{2}{P}\right)^2 . \omega_{se} \times 10^{-6}\right] . \omega_{se}\, MJ \quad (24)$$

$$KE = \frac{1}{2} M\omega_{se}\text{MJ} \quad (25)$$

Where M is moment of inertia in MJ.sec/elect.radian given as equation (26) (Das 2006; Kothari & Nagrath, 2008):

$$M = \left[\left(J\left(\frac{2}{P}\right)^2.\omega_{se} \times 10^{-6}\right]\right. \quad ' \quad (26)$$

The inertia constant H in in MJ/MVA or MW-sec/MVA, three phase MVA rating G and KE of the rotor of a synchronous machine are related by the expression of equation (27) from which equations (28) and (29) are obtained (Das 2006; Kothari & Nagrath, 2008):

$$GH = KE = \frac{1}{2}M\omega_{se}\text{MJ} \quad (27)$$

$$M = \frac{2GH}{\omega_{se}} = \frac{2GH}{2\pi f} = \frac{GH}{\pi f}\text{ MJ. Sec/elect. radian} \quad (28)$$

$$M = \frac{GH}{180f}\text{ MJ. Sec/elect.degree} \quad (29)$$

By expressing equations (28) and (29) in per unit with G assumed as base value, equations (30) and (31) give the expressions for M in electrical radian and electrical degree respectively (Das 2006; Kothari & Nagrath, 2008):

$$M_{(PU)} = \frac{H}{\pi f}sec^2/elect.radian \quad (30)$$

$$M_{(PU)} = \frac{H}{180f}sec^2/elect.degree \quad (31)$$

Formulation of Swing Equation

According to the Newton's second law, the motion of the rotor of a generating unit comprising a three-phase synchronous generator and its prime mover is described by equation (32) (Glover & Sarma, 2002; Kothari & Nagrath, 2008):

$$J \propto_m (t) = T_m(t) - T_e(t) = T_a(t) \quad (32)$$

Where $\propto_m$, T_m, T_e and T_n denote rotor angular acceleration in $rad/_{S^2}$, mechanical torque of the prime mover minus retarding torque resulting from mechanical losses in Nm, electrical torque responsible for the generator's total three-phase electrical power output plus electrical losses in Nm and net accelerating torque in Nm respectively.

The angular acceleration of the rotor is expressed by equation (33) (Glover & Sarma, 2002; Kothari & Nagrath, 2008):

$$\propto_m (t) = \frac{d\omega_m}{dt} = \frac{d^2\theta_m(t)}{dt^2} \quad (33)$$

With $\omega_m(t) = \frac{d\theta_m(t)}{dt}$ (34)

Where ω_m and θ_m respectively denote angular velocity of rotor in $rad/_S$ and angular position of rotor with respect to a stationary axis.

The operation of the generator requires that both T_m and T_e are positive while at steady-state, T_m is same as T_e, leading to T_a and $\propto_m$ being zero and consequently results in a constant velocity of the rotor termed synchronous speed. T_a is positive when T_m exceeds T_e, making $\propto_m$ to be positive and therefore, leads to an increased speed of the rotor. Equally, the speed of the rotor decreases when T_m is lower than T_e. Since, the angular

position of the rotor is conveniently measured with respect to a synchronously rotating reference axis unlike a stationary axis, $\theta_m(t)$ is, hence, $\theta_m(t) = \omega_{msyn}t + \delta_m(t)$

Where ω_{msyn} and δ_m are respectively defined as the rotor's synchronous angular velocity in $^{rad}/_{s}$ expressed as equation (35) (Glover & Sarma, 2002; Kothari & Nagrath, 2008):

(35)

and the angular position of the rotor with respect to a synchronously rotating reference.
The use of equations (33) and (35) in (32), produces equation (36):

$$J\frac{d^2\theta_m(t)}{dt^2} = J\frac{d^2\delta_m(t)}{dt^2} = T_m(t) - T_e(t) = T_a(t) \quad (36)$$

Multiplication of equation (36) by $\omega_m(t)$ and dividing by S_{rated} yields the generator's three-phase volt-ampere rating expressed by equation (37) which is a per-unit power quantity (Glover & Sarma, 2002; Kothari & Nagrath 2009):

$$\frac{J}{S_{rated}}\frac{d^2\delta_m(t)}{dt^2}\omega_m(t) = \frac{(T_m(t)-T_e(t))}{S_{rated}}\omega_m(t) = \frac{P_m(t)-P_e(t)}{S_{rated}} = P_{mp.u.}(t) - P_{ep.u.}(t) = P_{ap.u.}(t) \quad (37)$$

Where $P_{mp.u.}$ and $P_{ep.u.}$ denote prime mover's mechanical power mover minus mechanical losses in per unit and generator's electrical power output plus electrical losses in per unit.

Combining equation (37) with a normalized inertia constant, H defined as equation (38) results in equation (39) (Glover & Sarma, 2002; Kothari & Nagrath 2009):

$$H = \frac{J\omega_{msyn}^2}{S_{rated}} {}^{joules}/_{VA}\ or\ per\ unit - seconds \quad (38)$$

$$2H\frac{\omega_m(t)}{\omega_{msyn}^2}\frac{d^2\delta_m(t)}{dt^2} = P_{mp.u.}(t) - P_{ep.u.}(t) = P_{ap.u.}(t) \quad (39)$$

Considering that the per-unit angular velocity of the rotor is defined as equation (40) and substituted into equation (39), equation (41) is obtained (Glover & Sarma, 2002; Kothari & Nagrath 2009):

$$\omega_{p.u}(t) = \frac{\omega_m(t)}{\omega_{msyn}} \quad (40)$$

$$\frac{2H\omega_{p.u.}(t)}{\omega_{msyn}}\frac{d^2\delta_m(t)}{dt^2} = P_{mp.u.}(t) - P_{ep.u.}(t) = P_{ap.u.}(t) \quad (41)$$

Electrical angular acceleration α, electrical radian frequency ω, power angle δ of a synchronous generator with P number of poles, synchronous electrical radian frequency ω_{syn} and per-unit electrical frequency $\omega_{p.u}(t)$ are respectively expressed as equation (42) to (46) (Glover & Sarma, 2002; Kothari & Nagrath 2009):

$$\alpha(t) = \frac{P}{2}\alpha_m(t) \quad (42)$$

$$\omega(t) = \frac{P}{2}\omega_m(t) \quad (43)$$

$$\delta(t) = \frac{P}{2}\delta_m(t) \quad (44)$$

$$\omega_{syn} = \frac{P}{2}\omega_{msyn} \quad (45)$$

$$\omega_{p.u}(t) = \frac{\omega(t)}{\omega_{syn}} = \frac{\frac{2}{P}\omega(t)}{\frac{2}{P}\omega_{syn}} = \frac{\omega_m(t)}{\omega_{myn}} \quad (46)$$

The use of equations (44) to (45) in equation (41) results into equation (47) referred to as per-unit swing equation.

$$\frac{2H}{\omega_{syn}}\omega_{p.u.}(t)\frac{d^2\delta(t)}{dt^2} = P_{mp.u.}(t) - P_{ep.u.}(t) = P_{ap.u.}(t) \quad (47)$$

Equation (47) is very crucial in the analysis of rotor dynamics for transient stability studies. It is a second order ordinary differential equation in which the assumptions of lossless machine and negligible damper winding torque have eliminated the damping term (proportional to $\frac{d\delta}{dt}$) (Kothari & Nagrath, 2008). The electrical power P_e in equation (47) depends on the sine of angle δ and it mathematically expressed as equations (48) and (49) (Kothari & Nagrath, 2008):

$$P_e = P_{max}sin\delta \quad (48)$$

$$P_e = \frac{|E||V|}{X_d}sin\delta \quad (49)$$

Where $P_{max} = \frac{|E||V|}{X_d}$ (50)

Using equations (48) and (49) in equation (47), equations (51) and (52) are obtained respectively:

$$\frac{2H\omega_{p.u.}(t)}{\omega_{syn}}\frac{d^2\delta(t)}{dt^2} = P_{mp.u.}(t) - P_{maxp.u.}sin\delta(t) \quad (51)$$

$$\frac{2H\omega_{p.u.}(t)}{\omega_{syn}}\frac{d^2\delta(t)}{dt^2} = P_{mp.u.}(t) - \frac{|E||V|}{X_d}sin\delta(t) \quad (52)$$

With ω_{syn} assumed equal to $2\pi f$ and $\omega_{p.u.}(t)$ to unity for ease of analysis, the swing equations expressed by equations (51) and (52) are respectively modified as equations (53) and (54) respectively:

$$\frac{H}{\pi f}\frac{d^2\delta(t)}{dt^2} = P_{mp.u.}(t) - P_{maxp.u.}sin\delta(t) \quad (53)$$

$$\frac{H}{\pi f}\frac{d^2\delta(t)}{dt^2} = P_{mp.u.}(t) - \frac{|E||V|}{X_d}sin\delta(t) \quad (54)$$

Numerical Solution of Swing Equation

Swing equation is a non-linear second-order differential equation and for easy handling during transient stability analysis, it requires linearization via numerical iterative procedure since exact solution is difficult in practice. The common numerical techniques available for solving the swing equation are Euler, modified Euler, classical Runge-Kutta and point-to-point methods (Conlon, 2003; Kothari & Nagrath, 2008; Ogboh *et al.*, 2018). But for the purpose of this study, modified Euler method (MEM) was adopted because of simplicity and directness with

which a good approximation of non-linear system can be obtained with a very small step size.

Modified Euler Numerical Solution of Swing Equation

The linearization of swing equation via MEM requires that equation (47) modified as equations (53) and (54) be transformed into state variable forms for easy analysis. The k[th] generator swing equation and the state variable formulations are defined by equations (55)-(61) (Das, 2006):

$$\frac{d^2\delta_k}{dt^2} = \frac{\pi f}{H_k}\left(P_{Gk}^0 - P_{Gk}\right); k = 1,2,\cdots,m \quad (55)$$

$$x_{1k} = \delta_k = \angle E_k' \quad (56)$$

$$x_{2k} = \dot{\delta}_k \quad (57)$$

Then

$$\dot{x}_{1k} = x_{2k} \quad (58)$$

$$\dot{x}_{2k} = \frac{\pi f}{H_k}\left(P_{Gk}^0 - P_{Gk}\right); k = 1,2,\cdots,m \quad (59)$$

Initial state vector upon occurrence of fault are defined by equations (63) and (64):

$$x_{1k}^0 = \delta_k^0 = \angle E_k^0 \quad (60)$$

$$x_{2k=0}^0 \quad (61)$$

The computational algorithm involved in solving the swing equation (55) expressed by state variable forms of equations (56) to (61) via the MEM is detailed as follows:

Step 1. Perform power flow analysis prior to disturbance with specified voltages and powers.

Step 2. Estimate the voltage behind transient reactances of generators (E_k^0) from equation (62):

$$E_{Gi}' = V_{Gi}^0 - jX'_{Gk}I'_{Gk} \quad (62)$$

The generator e.m.f magnitudes and initial rotor angle are fixed by this (reference or slack bus voltage V_1^0).

Step 3. Compute, Y_{BUS} (during fault, post fault, line reclosed).

Step 4. Specify iteration count $r = 0$.

Step 5. Compute generator power outputs via appropriate Y_{BUS} using general active power equation (63):

$$P_1 = |E_1'|^2 G_{11} + |E_1'||E_2'||Y_{12}|cos(\delta_1 - \delta_2 - \theta_{12}) \quad (63)$$

This gives $P_{Gk}^{(r)}$ for $t = t^{(r)}$.

Step 6. Estimate $\left[\left(\dot{x}_{1k}^{(r)}, \dot{x}_{2k}^{(r)}\right), k = 1,2,\cdots,m\right]$ from equation (64):

$$\dot{x}_{2k} = \frac{\pi f}{H_k}\left(P_{Gk}^0 - P_{Gk}\right); k = 1,2,\cdots,m \quad (64)$$

Step 7. Determine the first state estimates for $t = t^{(r+1)}$ from equations (65) and (66):

$$x_{1k}^{(r+1)} = x_{1k}^{(r)} + \dot{x}_{1k}^{(r)}\Delta t\,, \;\; k = 1,2,\cdots m \tag{65}$$

$$x_{2k}^{(r+1)} = x_{2k}^{(r)} + \dot{x}_{2k}^{(r)}\Delta t \tag{66}$$

Step 8. Determine the first estimates of $E_k^{(r+1)}$ from equation (67):

$$E_k^{(r+1)} = E_k^0\left(cosx_{1k}^{(r+1)} + jsinx_{1k}^{(r+1)}\right) \tag{68}$$

Step 9. Determine $P_{Gk}^{(r+1)}$ using appropriate Y_{BUS} and equation (69):

$$\delta_n = \delta_{n-1} + \Delta\delta_n \tag{69}$$

Step 10. Compute $\left[\left(\dot{x}_{1k}^{(r+1)}, \dot{x}_{2k}^{(r+1)}\right), k = 1,2,\cdots,m\right]$ from equation (70):

$$\dot{x}_{2k} = \frac{\pi f}{H_k}\left(P_{Gk}^0 - P_{Gk}\right); k = 1,2,\cdots,m \tag{70}$$

Step 11. Determine the average values of state derivatives from equations (71) and (72):

$$\dot{x}_{1k,\ avg}^{(r)} = \frac{1}{2}\left[\dot{x}_{1k}^{(r)} + \dot{x}_{1k}^{(r+1)}\right] \quad k = 1,2,\cdots m \tag{71}$$

$$\dot{x}_{2k,\ avg}^{(r)} = \frac{1}{2}\left[\dot{x}_{2k}^{(r)} + \dot{x}_{2k}^{(r+1)}\right] \tag{72}$$

Step 12. Compute the final state estimates for $t = t^{(r+1)}$ from equations (73) and (74):

$$x_{1k}^{(r+1)} = x_{1k}^{(r)} + \dot{x}_{1k,\ avg}^{(r)}\Delta t \quad k = 1,2,\cdots m \tag{73}$$

$$x_{2k}^{(r+1)} = x_{2k}^{(r)} + \dot{x}_{2k,\ avg}^{(r)}\Delta t \tag{74}$$

Step 13. Obtain the final estimate for E_k at $t = t^{(r+1)}$ using equation (75):

$$E_k^{(r+1)} = \left|E_k^0\right|\left(cosx_{1k}^{(r+1)} + jsinx_{1k}^{(r+1)}\right) \tag{75}$$

Step 14. Print $\left(x_{1k}^{(r+1)}, x_{2k}^{(r+1)}\right); k = 1,2\cdots,m$ (76)

Step 15. Test for time limit (time for which swing curve is to be plotted), i.e., check if $r > r_{final}$. If not, $r = r + 1$ and repeat from step 5 above. Otherwise print results and stop.

Power Flow Model of STATCOM for Transient Stability Improvement

The power flow equations guiding the operation of STATCOM as voltage source converter are expressed by equations (77) to (81) with matrix in equation (82) giving the linearized Newton-Raphson model of STATCOM applying these equations (Acha *et al.*, 2004).

$$E_{vR} = V_{vR}(cos\delta_{vR} + jsin\delta_{vR}). \quad (77)$$

$$P_{vR} = V_{vR}^2 G_{vR} + V_{vR}V_k[G_{vR}cos(\delta_{vR} - \theta_k) + B_{vR}sin(\delta_{vR} - \theta_k)] \quad (78)$$

$$Q_{vR} = -V_{vR}^2 B_{vR} + V_{vR}V_k[G_{vR}sin(\delta_{vR} - \theta_k) + B_{vR}cos(\delta_{vR} - \theta_k)] \quad (79)$$

$$P_k = V_k^2 G_{vR} + V_k V_{vR}[G_{vR}cos(\theta_k - \delta_{vR}) + B_{vR}sin(\theta_k - \delta_{vR})] \quad (80)$$

$$Q_k = -V_k^2 B_{vR} + V_k V_{vR}[G_{vR}sin(\theta_k - \delta_{vR}) + B_{vR}cos(\theta_k - \delta_{vR})] \quad (81)$$

$$\begin{bmatrix} \Delta P_k \\ \Delta Q_k \\ \Delta P_{vR} \\ \Delta Q_{vR} \end{bmatrix} = \begin{bmatrix} \frac{\partial P_k}{\partial \theta_k} & \frac{\partial P_k}{\partial |V_k|}|V_k| & \frac{\partial P_k}{\partial \delta_{vR}} & \frac{\partial P_k}{\partial |V_{vR}|}|V_{vR}| \\ \frac{\partial Q_k}{\partial \theta_k} & \frac{\partial Q_k}{\partial |V_k|}|V_k| & \frac{\partial Q_k}{\partial \delta_{vR}} & \frac{\partial Q_k}{\partial |V_{vR}|}|V_{vR}| \\ \frac{\partial P_{vR}}{\partial \theta_k} & \frac{\partial P_{vR}}{\partial |V_k|}|V_k| & \frac{\partial P_{vR}}{\partial \delta_{vR}} & \frac{\partial P_{vR}}{\partial |V_{vR}|}|V_{vR}| \\ \frac{\partial Q_{vR}}{\partial \theta_k} & \frac{\partial Q_{vR}}{\partial |V_k|}|V_k| & \frac{\partial Q_{vR}}{\partial \delta_{vR}} & \frac{\partial Q_{vR}}{\partial |V_{vR}|}|V_{vR}| \end{bmatrix} \begin{bmatrix} \Delta\theta_k \\ \frac{\Delta|V_k|}{|V_k|} \\ \Delta\delta_{vR} \\ \frac{\Delta|V_{vR}|}{|V_{vR}|} \end{bmatrix} \quad (82)$$

Where E_{vR}, V_{vR}, δ_{vR}, P_{vR}, Q_{vR}, P_k, Q_k, V_k and θ_k respectively denote variable voltage source, controllable voltage magnitude, source phase angle, active power supplied by the shunt converter, reactive power supplied by the shunt converter, active power at bus *k*, reactive power at bus *k* , voltage at bus *k* and voltage phase angle at bus *k*.

The elements of the Jacobian matrix in equation (82) are derived by the partial differential manipulation of equations (78) to (81) with respect to θ_k, V_k, δ_{vR} and V_{vR} as the state variables.

The STATCOM operation for improvement of transient stability can be described using with three Cases of the swing equation (Kakaiya & Parekh, 2019):

Case 1: When $P_m = P_e$, the accelerating power is zero and the system is in steady state.

Case 2: When $P_m > P_e$, the rotor accelerates due to the loss of a large load.

Case 3: $P_m < P_e$, the rotor's acceleration decreases as a result of three-phase fault occurrence.

For the control of the machine's output power, when H changes, the accelerating power is controlled with the limits. If scenario 2 occurs, the machine accelerates and the STATCOM generates a voltage and introduces a capacitive reactance in the line. However, for scenario 3, the machine experiences retardation and STATCOM operates in such a way that it produces a voltage that causes inductive reactance to be introduced into the line.

Test Network and Simulation

This work considered two standard power system network models as test cases. These models include IEEE 3-machine, 9-bus power system and IEEE 5-machine, 14-bus power system with one-line diagram of the systems respectively presented in Figures 2 and 3 while the data are provided in Appendices I-VI.

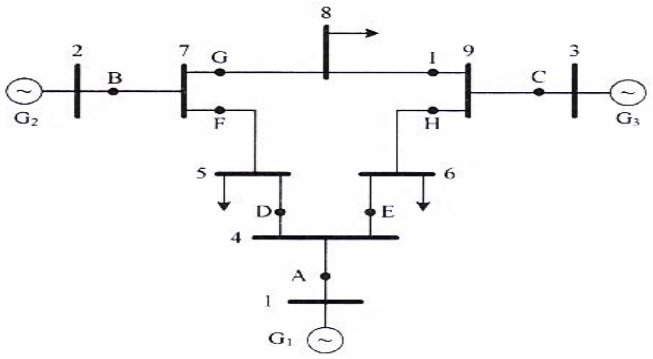

Figure 2: IEEE 3-machine, 9-bus power network

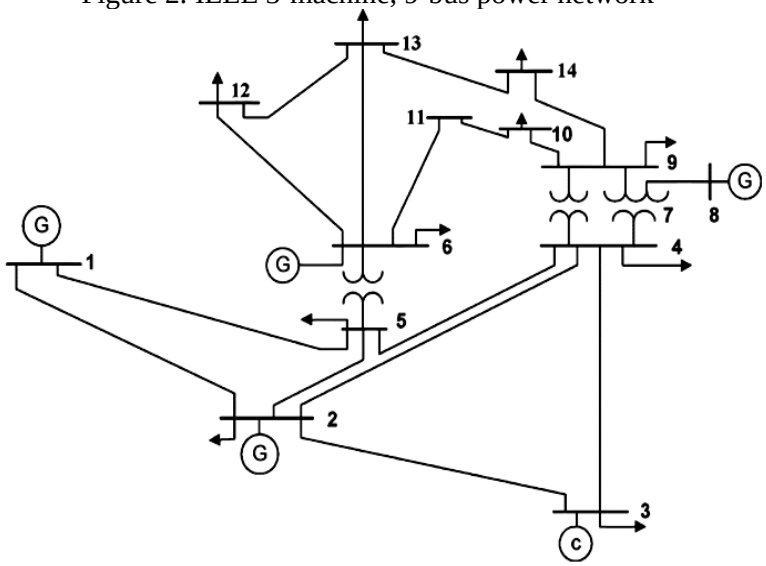

Figure 3: IEEE 5-machine, 14-bus power network

The transient stability simulations of the two networks were carried out via codes developed in MATLAB environment which is robust and has high capacity for handling mathematical algorithms. The bus, branch and generator data of the networks with STATCOM's rating were used as input variables during simulations. The systems' responses with and without STATCOM when a balanced three-phase short-circuit was introduced on some buses as transient disturbance were examined and the critical fault clearing times (CFCTs) were determined.

RESULTS AND DISCUSSION

IEEE 3-Machine, 9-Bus Network Load Flow and Transient Stability Results

IEEE 9-Bus Network Load Flow Results

The load flow results on the IEEE 9-bus network prior to analysis and enhancement of transient stability on the system are presented in Figures 4 and 5. The voltage profile in Figure 4 revealed that all the buses in the system had their voltage magnitudes within the acceptable voltage tolerance limit of 0.95 to 1.1 p.u. STATCOM inclusion in the system further enhanced the bus 5 voltage magnitude from 0.9956 to 0.9985 p.u. which represents 0.29% increase. Figure 5 revealed that without STATCOM, the system total active power loss was 4.641 MW while the

value reduced to 4.600 MW with compensation applied to give a further 0.88% improvement in the active power flow of the system. These results are indication that before the application of enhancement on the IEEE 9-bus network, the system was operating effectively as no bus infringed the pre-defined voltage tolerance limit to create instability. The introduction of STATCOM further enhanced the system stability by improving the voltage on one of the buses while the others maintained their voltage magnitudes. The effect of the stabilized system voltage reflected on the active power loss observed, being of lower magnitude and further decreased with the compensation applied. As a result, bus 8 was selected to examine the impact of introduction of a major disturbance in the form of a balanced three-phase short-circuit fault on the system performance with and without enhancement.

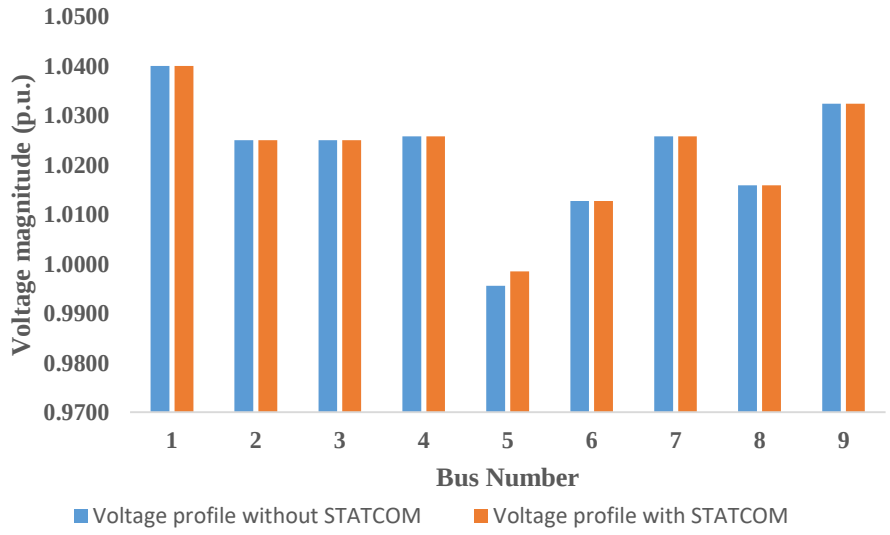

Figure 4: voltage magnitudes of the IEEE 9-bus network

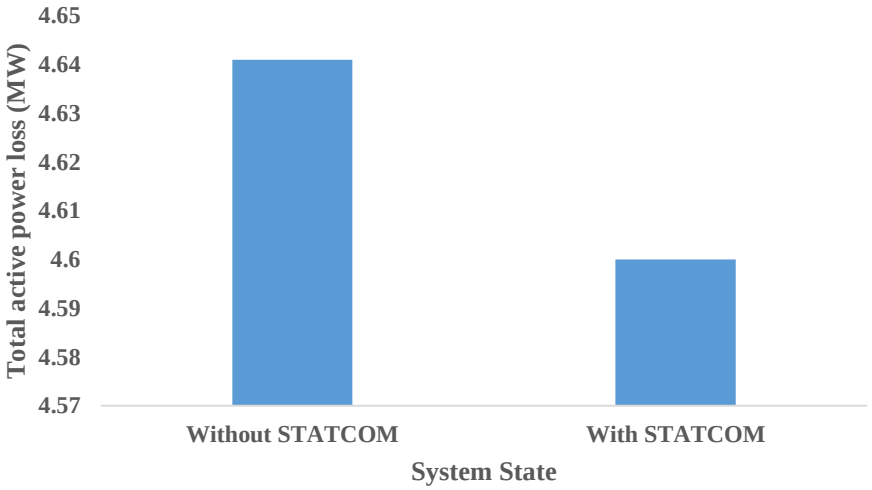

Figure 5: Total active power loss of IEEE 9-bus network.

IEEE-9 Bus Network Transient Stability Analysis and Enhancement Results for Three-Phase Fault on Bus 8, Line [7-8]

The swing curves of the generators in IEEE 9-bus network for three-phase short circuit fault introduced on bus 8, line [7-8] and cleared at

different times with and without STATCOM are presented in Figures 6 to 9. At fault clearing time (FCT) of 0.20 s, the swing curves in Figures 6a and b showed that the system was stable before and after compensation. FCT increase to 0.21 s without STATCOM resulted in out of step of the rotor angular difference of generator 2 with respect to the reference generator, signifying that generator 2 had lost stability while generator 3 maintained stability as shown in Figure 7a. The use of STATCOM on bus 8, line [7-8], however, restored generator 2 back to stability along with generator 3 that sustained its synchronism as depicted in Figure 7b.

FCT increase to 0.27 s with no STATCOM application led to the rotor angular difference of generator 3 with respect to the reference generator increasing indefinitely, suggesting that generator 3 in addition to generator 2 had gone out of step as Figure 8a shows.

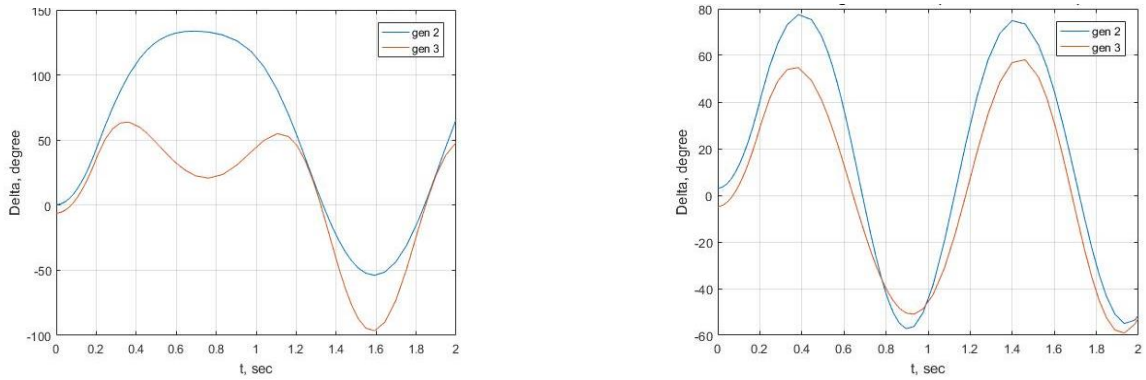

(a) (b)

Figure 6: Swing curve of three-phase fault on bus 8, line [7-8] of IEEE-9 bus power network and cleared at 0.2 s (a) without STATCOM and (b) with STATCOM

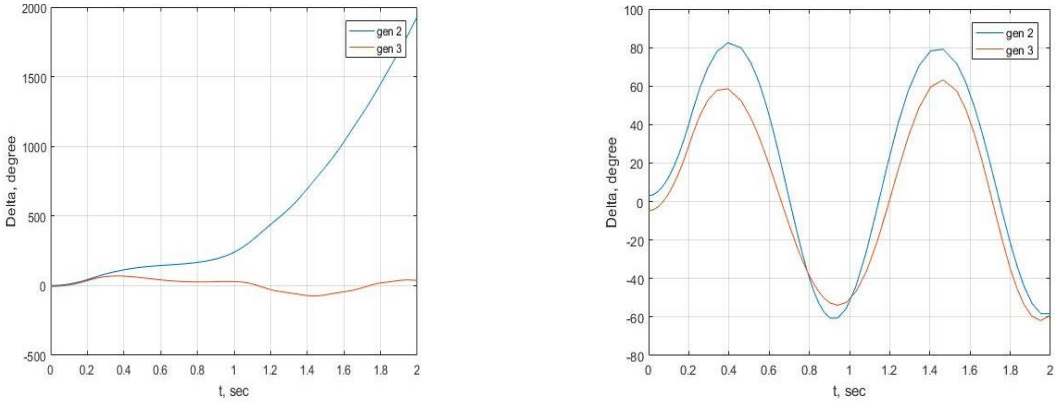

(a) (b)

Figure 7: Swing curve of three-phase fault on bus 8, line [7-8] of IEEE-9 bus power network and cleared at 0.21 s (a) without STATCOM (b) with STATCOM

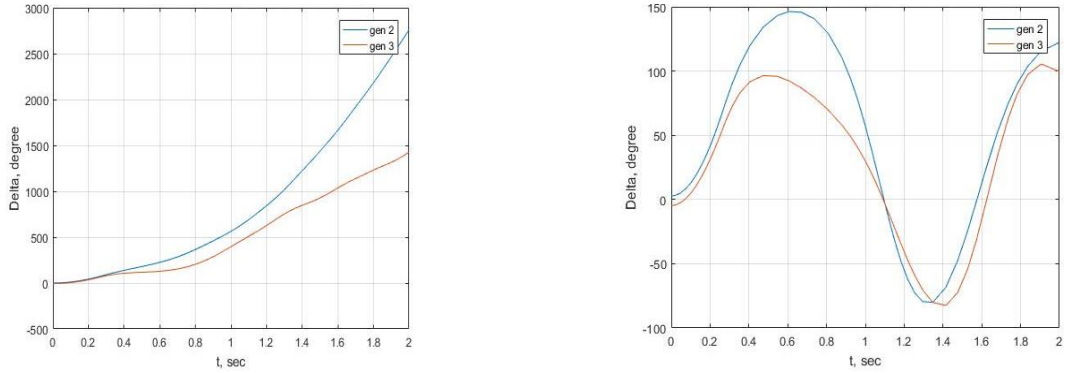

(a) (b)

Figure 8: Swing curve of three-phase fault on bus 8, line [7-8] of IEEE-9 bus power network and cleared at 0.27 s (a) without STATCOM (b) with STATCOM

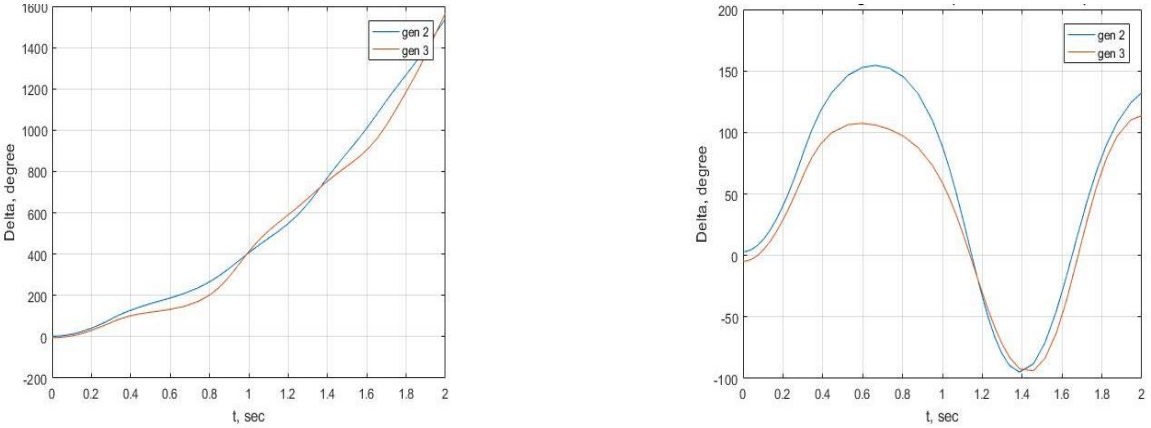

(a) (b)

Figure 9: Swing curve of three-phase fault on bus 8, line [7-8] of IEEE-9 bus power network and cleared at 0.30 s (a) without STATCOM (b) with STATCOM

Installation of STATCOM in the network at bus 8, however, aided the restoration of generators 2 and 3 back to stability as observed from Figure 8b. It was, therefore, inferred from Figures 8a and 9a that generators 2 and 3 had a respective CFCT of 0.20 and 0.21 s. This implication of these fault clearing times is that beyond these times, the phase angle difference of both generators 2 and 3 with respect to the reference generator will undergo indefinite increase without compensation. Increase in FCT margin to 0.30 s showed instability persisted on both generators 2 and 3 without STATCOM as shown in Figure 9a but with STATCOM installation, both generators regained stability as Figure 9b depicts.

Analysis of the obtained transient stability results for IEEE 9-bus power network indicated that STATCOM's integration into the system enhanced the CFCT in such a way that the stability of the system was sustained in the event of the introduction of the balanced three-phase short-circuit fault. STATCOM was able to maintain the system synchronous operation through compensation of reactive power in the vicinity of the fault introduction where var was deficient. Due to this action of the controller, the negative impact of the fault was mitigated and the system was stabilized through the maintenance of synchronous operation depicted by the continuous undulating effect of the swing curves.

IEEE 5-Machine, 14-Bus Power Network Load Flow and Transient Stability Results

IEEE 14-Bus Network Load Flow Results

The results of IEEE 14-bus network load flow study prior transient stability analysis and enhancement are presented in Figures 10 and 11

which respectively show system voltage profile and total active. Observation from Figure 10 revealed that all the buses in the system had their voltage magnitudes within the acceptable voltage tolerance limit of 0.95 to 1.1 p.u. The STATCOM application enhanced the voltage magnitudes of buses 4 and 9 to from 1.0248 to 1.0300 and 1.0240 to 1.035 p.u. which represent increase of 0.5 and 0.6%, respectively. According to Figures 11, the system total active which was 13.514 MW without compensation reduced to 13.014 MW with compensation, leading to 3.7% improvement in the active power flow. These results signified that IEEE 14-bus power network was effectively operating with stabilized bus voltages and minimized active power loss before compensation and it performance was further enhanced when STATCOM was applied.

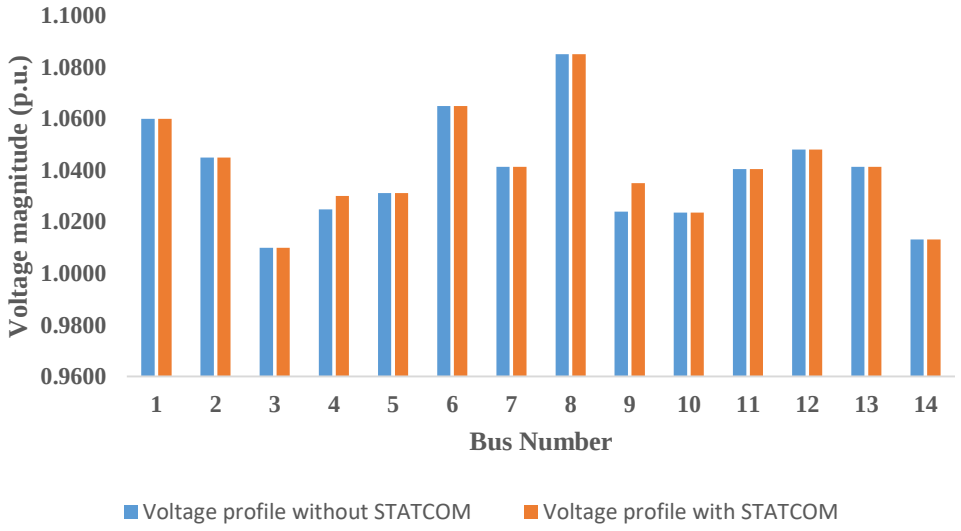

Figure 10: Voltage magnitudes of the IEEE 14-bus network

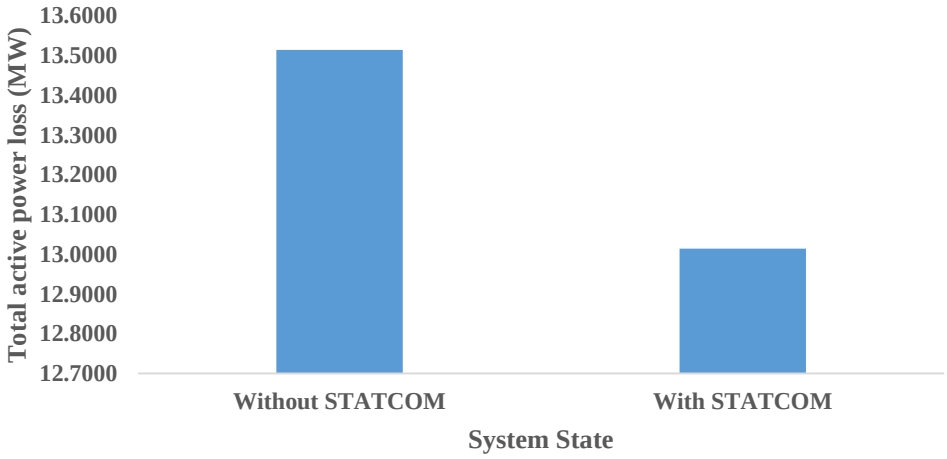

Figure 11: Total active power loss of the IEEE 14-bus network.

Taking into cognizance that no bus within the network violated the specified voltage limit based on the results of load flow, bus 6 was selected to investigate the effect of transient disturbance on the network with and without compensation.

IEEE 14-Bus Network Transient Stability Analysis and Enhancement Results for Three-Phase Fault on Bus 6, Line [5-6]

The swing curves of generators in the IEEE 14-bus power network for three-phase short circuit

fault introduced on bus 6, line [5-6] and cleared at different times with and without STATCOM are presented in Figures 12 to 14. The swing curves in Figures 12a and b for fault on bus 6, line [5-6] which was cleared at 0.36364 s showed that system was stable before and after compensation. FCT increase to 0.36365 s without STATCOM as observed from Figure 13a resulted in system instability, with generators 2 to 5 losing synchronism for indefinite decrease in the respective rotor angular difference with respect to the reference generator. The system, however, regained synchronism when STATCOM was installed as shown in Figure 13b.

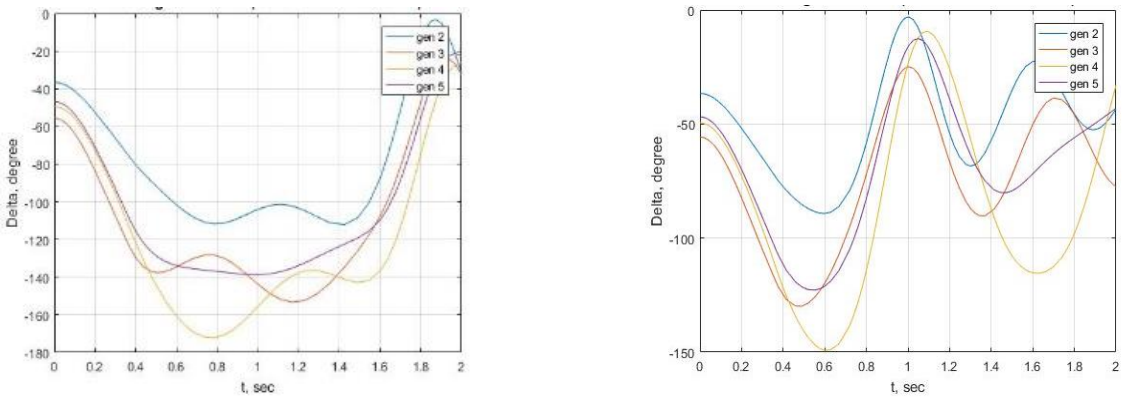

(a) (b)

Figure 12: Swing curve of three-phase fault on bus 6, line [5-6] of the IEEE 14-bus power network and cleared at 0.36364 s (a) without STATCOM (b) with STATCOM

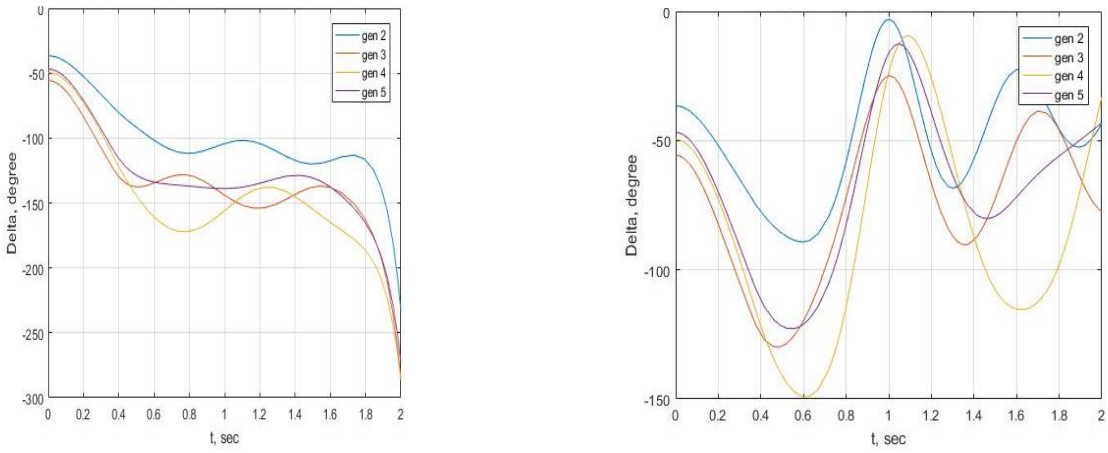

(a) (b)

Figure 13: Swing curve of three-phase fault on bus 6, line [5-6] of the IEEE 14-bus power network and cleared at 0.36365 s (a) without STATCOM and (b) with STATCOM

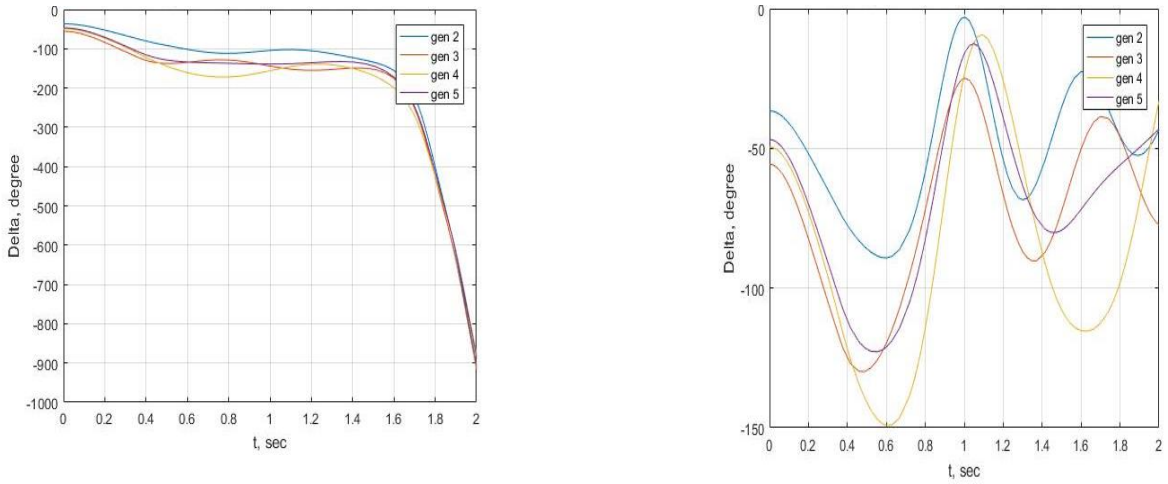

Figure 14: Swing curve of three-phase fault on bus 6, line [5-6] of the IEEE 14-bus power network and cleared at 0.36366 s (a) without STATCOM (b) with STATCOM.

A further increase in FCT to 0.36366 s without enhancement showed that the loss of synchronism observed on the system's generators 2 to 5 was sustained as Figure 14a depicts. Stability was later restored into the network with application of STATCOM as presented in Figure 14b. Analysis of the obtained results indicated that the CFCT of generators 2 to 5 without compensation is 0.36364 s. The introduction of enhancement via STATCOM maintained the stability of the system beyond a FCT of 0.36365 s where generators 2 to 5 had all lost synchronism. The obtained transient stability results indicated that the use of STATCOM on IEEE 14-bus power network delayed the CFCT such that the system did not lose synchronism the balanced three-phase short-circuit fault application which was reflected in the continuous undulating effect of the swing curves.

Discussion of the Results

This study dealt with transient stability assessment of two different power grid models namely IEEE 9-bus and 14-bus power networks with and without compensation. Prior to transient stability analysis, load flow was performed on each grid to examine their steady state performance before and after compensation. The load flow results revealed that both networks had voltage magnitudes within the specified voltage tolerance limit with and without compensation; an indication the systems were operating optimally. STATCOM inclusion on the grids further enhanced the systems' bus voltage magnitudes which were already within the acceptable limit and the active power also improved. The voltage profile and power loss improvements could be attributed to the robust compensating capability of the device. STATCOM was able to inject reactive power into the network to compensate reactive power at different points where there were deficiencies as a result of fault applied and voltages at these points improved and were within the desired range with minimized total active power loss.

Having examined the steady state conditions of the IEEE 9-bus and 14-bus power grids before and after compensation, transient stability analysis was carried on selected buses. The three-phase short circuit fault introduced on bus 8, line [7-8] of the IEEE 9-bus grid and cleared at 0.169 s revealed that the system was stable with and without STATCOM but FCT increase to 0.17 s resulted in instability of the system which was sustained till 0.2 s. Introduction of STATCOM, however, mitigated the instability and the

undulating characteristics of the rotor angle-time ($\delta - t$) relationship restored.

Similarly, the clearing of the balanced three-phase short-circuit fault introduced on bus 6, line [5-6] of IEEE 14-bus power network at 0.36364 s revealed that the system was stable with and without STATCOM. The FCT delay up to 0.36365 s led to system instability where generators 2 to 5 went out of step and the instability was sustained till a FCT of 0.36366 s without STATCOM. STATCOM inclusion enhanced the stability of the system beyond 0.36366 s where generators 2 to 5 had all lost synchronism when three-phase short circuit fault introduced on bus 6, line [5-6] of the grid. The implication of the obtained results is that STATCOM application on IEEE 9-bus and IEEE 14-bus power networks was able to sustain systems' stability following the fault introduction. This was made possible via reactive power compensation offered by the device and eventually extended the time for fault clearance.

The results of transient stability analysis and improvement in this study are consistent with the findings of Abbas *et al.* (2021), and Barsoum *et al.* (2018). The works of Abbas *et al.* (2021) revealed that critical clearing time is a key and decisive factor that determines whether a system maintains or loses stability in the event of major or large disturbance such as fault. Barsoum *et al.* (2018) discovered in his findings that STATCOM application was an appropriate technique in curtailing transient instability of the test network considered. These submissions from the two authors are in consonant with the results obtained from the present study where it was found out that CFCT of fault was crucial for sustenance of stability of the considered power networks when no compensation was applied during fault simulation and that due to the compensating ability of STATCOM, the CFCT of the considered systems was extended and stability maintained in the event of fault introduction.

CONCLUSION

Persistent increase in loading of the long transmission lines which are already overburdened than the initial designed capacity has made transient stability an important factor in the transfer of electric power following a major disturbance. Transient stability is a very important tool use to diagnose the systems so as to ensure that synchronism is not lost. In this work, transient stability improvement through STATCOM was carried out on the IEEE 9-bus and 14-bus power grids. Power flow and swing equations modelling the performance under steady state and transient condition were formulated and simulated via codes developed in MATLAB environment with and without enhancement.

The power flow result revealed that no bus in the considered networks violated the voltage tolerance limit before and after STATCOM was applied. The δ-*t* characteristics of the generators in the two networks considered revealed that sustenance of synchronism is a function of CFCT and the compensation provided by STATCOM when a balanced three-phase short-circuit fault was introduced on the selected buses. Furthermore, delay in FCT caused some of the generators which were initially stable to become unstable when STATCOM was not used on the system. However, the use of STATCOM on different selected buses on the two networks generally enhanced the stability of the system beyond the point at which synchronism was lost when CFCT was exceeded as a result of the reactive power compensation provided by the STATCOM. Based on the result of this research, STATCOM was able to provide the needed enhancement for transient stability improvement of the considered power networks.

As a suggestion for future works in this research area, comparative evaluation between STATCOM and other versatile FACTS controllers including SSSC, SVC, IPFC, TCSC and UPFC for transient stability enhancement

could be conducted to gain more useful insights into the deployment of devices. carried out. More so, the use of optimization approaches such as fuzzy logic, genetic algorithm, artificial neural network, particle swarm optimization among others could be considered for optimal allocation of the FACTS controllers for transient stability improvement in power system networks.

REFERENCES

Abbas, A., Doud, K.R., & Ahmed, E.S.A. (2021). Power System Transient Stability Case Study: A Power Sub-Station Plant in Sudan. *World Scientific News*, *158*, 267-284.

Acha, E., Fuerte-Esquivel, C.R., Ambriz-Pe'rez, H., & Angeles-Camacho, C., 2004. FACTS: Modelling and Simulation in Power Networks. John Wiley and Sons Limited, West Sussex, England.

Adebisi, O.I., Adejumobi, I.A., Ogunbowale, P.E., & Ade-Ikuesan, O.O. (2018). Performance Improvement of Power System Networks Using Flexible Alternating Current Transmission Systems Devices: The Nigerian 330 kV Electricity Grid as a Case Study. *LAUTECH Journal of Engineering and Technology*, *12*(2), 46-55.

Alhamrouni, I., Rasyid, I., Salem, M., Ismail, B., Jusoh, A., & Sutikno, T. (2020). Integration of STATCOM and ESS for Power System Stability Improvement. *International Journal of Power Electronics and Drive System (IJPEDS), 11*(2), 859-869.

Asare, P., Diez, T., Gali, A, & Carillo, E. (1994). An Overview of Flexible AC Transmission System. Electrical and Computer Engineering Technical Report, School of Electrical Engineering, Purdue University, West Lafayette, Indiana, USA.

Barsoum, N., Zulkeffley, N., & Songkin, M. (2018). Transient Stability Simulation of 33 kV Power Grid. *Energy and Power Engineering*, *10*, 301-318.

Barua, P., Barua, R., Quamruzzaman, M., & Rabbani, M.G. (2021). Small Signal Stability and Transient Stability improvement of Bangladesh Power System using TCSC, SVC and TCSC, STATCOM based series shunt compensator. In *2021 IEEE International Conference on Science & Contemporary Technologies (ICSCT)*, pp. 1-5.

Conlon, F. (2003). Transient Stability Analysis Handbook. Dublin Institute of Technology, Dublin, Ireland.

Das, D. (2006). Electrical Power System. New Age International Publisher, New Delhi, India. 483pp.

Fadadu M., & Lotiya J. (2016). Comparison and Performance Analysis of Various FACTS Devices in Power System. *International Journal of Engineering and Computer Science. 5*(6), 16765-16771

Fan, B., Young, Q., Wang, K., Xu, J., & Sun, Y. (2016). Transient Stability Enhancement Control of Power System with Time-Varying Constraints. *IET Generation, Transmission & Distribution, 10*(13), 3251-3263.

Fathollahi, A., Kargar, A., & Derakhshandeh, S. Y. (2022). Enhancement of power system transient stability and voltage regulation performance with decentralized synergetic TCSC controller. *International Journal of Electrical Power & Energy Systems*, *135*, 107533.

Garg, L., & Khan, S. (2021). Application of FACTS Controller for Enhancement of Transient Stability. *In: Kumar, A., Mozar, S. (eds) ICCCE 2020. Lecture Notes in Electrical Engineering, Springer, Singapore*, *698*, 733-745.

Ghaedi, S., Abazari, S., & Markadeh, G.A. (2021). Transient Stability Improvement of Power System with UPFC Control by using Transient Energy Function and Sliding Mode Observer based on Locally Measurable Information. *Measurement*, *183*, 109842.

Glover, J.D., & Sarma, M. (2002). Power System Analysis and Design with Personal Computer Application., PWS-KENT

Publishing Company, Boston, USA. 963pp.

Gupta, J.B. (2011). A Course in Power Systems. S K Kataria and Sons, New Delhi, India.1600pp.

Gupta, K., & Pahariya, Y. (2017). Simulation Analysis of FACTS Devices for Transient Stability Improvement in Multi-Machine System, *International Journal of Current Trends in Engineering & Technology*, *3*(1): 16-20.

Gurijala, S.B., Kishore, D.R., Nittala, R., & Godala, R.R. (2021). Stability Analysis and Efficiency Improvement of IPFC using Latest PR Controller. *Archives of Electrical Engineering*, *70*(3), 615-630.

Hadi, S. (2008). Power System Analysis. McGrew-Hill Companies. Inc., New York, USA. 720pp.

Jokojeje, R.A., Adejumobi, I.A., Adebisi, O.I., & Mufutau, W.O. (2015a). Reactive Power Compensation in Nigeria Electricity Grid Using Static Synchronous Compensator (STATCOM). *International Organization of Scientific Research Journal of Electrical and Electronics Engineering*, *10*(2), 8-20.

Jokojeje, R.A. Adejumobi, I.A., Mustapha, A.O., & Adebisi, O.I. (2015b). Application of Static Synchronous Compensator (STATCOM) in Improving Power System Performance: A Case Study of the Nigeria 330 kV Electricity Grid. *Nigerian Journal of Technology*, *34*(3), 564-572.

Kakaiya, S. & Parekh, D.B. (2019). Transient stability Improvement Using STATCOM. *3rd International Conference on Advance in Power Generation from Renewable energy source*, pp. 1-9

Kothari, D.P., & Nagrath, I.J. 2008. Power System Engineering, Second Edition, Tata McGraw-Hill Publishing Company Limited, New Delhi, India. 1074pp.

Noaman, K., Haseeb, A., & Amjad, K. (2017). Transient Stability Enhancement of Power System Using UPFC. *International Journal of Engineering Works*, *4*(2), 33-40.

Mbae, M., & Nwulu, N. (2022) Impact of Hybrid FACTS Devices on the Stability of the Kenyan Power System. *International Journal of Electrical and Computer Engineering (IJECE)*, *12*(1), 12-21.

Narayana, G., & Gudapati, S.R. (2021) Recent Advances of STATCOM in Power Transmission Lines-A Review. *Turkish Journal of Computer and Mathematics Education*, *12* (3), 4621-4626.

Naveed, U., Muhammad, N.A., Uzair, M., Tanvir, A., & Nisar, A. (2019). Analysis Study of Different Control Schemes used for the Improvement of Transient Stability: A Review. *International Journal of Engineering Works*, *6*(10), 333-338.

Ogboh, V.C., Obute, K.C., & Anyalebechi, E.A. (2018). Transient Stability Analysis of Power Station (A Case Study of Nigeria Power Station). *The International Journal of Engineering and Science*, *7*(8), 28-42.

Praveen, K., Agrawal, S.D., & Arun, S. (2016). FACTS Devices Improvement of Power System Stability. *SSRG International Journal of Electrical and Electronics Engineering*, *3*(5), 117-120.

Radmehr, M., Khorasaninezhad, M., & Azizpour, A. (2017) Enhancing of Power System Transient Stability by Using Continuously Variable Braking Resistor (CVBR). *Journal of New Innovations in Electrical Engineering*, *2*, 102- 110

Sawkmie, D., Julene, S.H., Thabah, M.L., & Smriti, D. (2018). A Review on Stability Improvement of Wind Farm Using FACTS Devices. *ADBU Journal of Electrical and Electronics Engineering*, *2*(1), 17-21.

Sharan C, Subasangkari S, Ganesh V. N, & Ajay Danie J (2019) Research of Facts Devices for Stability.International Journal of Recent Technology & Engineering. 8: 1585-1590.

Shrivastava, M., Prakash, V., Kaushik, V., & Upadhyay, V.K. (2021). Transient Stability Improvement of IEEE 9-Bus System Using Static Var Compensator. *International Journal of Research in*

Engineering, Science and Management, *4*(4), 98-102.

Singh, R.K., & Singh, N.K. (2022). Power system transient stability improvement with FACTS controllers using SSSC-based controller. *Sustainable Energy Technologies and Assessments*, *53*, 102664.

APPENDICES

I: Bus Parameters for IEEE 9-bus Power Network

Bus No	Bus Type	Pd (MW)	Qd (MVAr)	Vm (p.u.)	Va (p.u.)	kVbase	Vmax(p.u)	Vmin (p.u)
1	3	0	0	1	0	16.5	1.1	0.95
2	2	0	0	1	0	18	1.1	0.95
3	2	0	0	1	0	13.8	1.1	0.95
4	1	0	0	1	0	230	1.1	0.95
5	1	125	50	1	0	230	1.1	0.95
6	1	90	30	1	0	230	1.1	0.95
7	1	0	0	1	0	230	1.1	0.95
8	1	100	35	1	0	230	1.1	0.95
9	1	0	0	1	0	230	1.1	0.95

II: Generator Parameters for IEEE 9-bus Power Network

Bus No	Pg (MW)	Qg (MVAr)	Qmax (Mvar)	Qmin (MVAr)	Vg (p.u)	Pmax (MW)	Pmin (MVAr)	X (p.u.)	H
1	0	0	300	-300	1.04	250	10	0.608	23.64
2	163	0	300	-300	1.025	300	10	0.1198	6.01
3	85	0	300	-300	1.025	270	10	0.1813	3.01

III: Branch Parameters for IEEE 9-bus Power Network

From Bus	To Bus	R (p.u.)	X (p.u.)	B (p.u.)
1	4	0	0.0576	0
4	6	0.017	0.092	0.158
6	9	0.039	0.17	0.358
3	9	0	0.0586	0
8	9	0.0119	0.1008	0.209
7	8	0.0085	0.072	0.149
7	2	0	0.0625	0
5	7	0.032	0.161	0.306
4	5	0.01	0.085	0.176

IV: Bus Parameters for IEEE 14-Bus Test System

Bus No	Bus Type	Pd (MW)	Qd (MVAr)	Vm (p.u.)	Va (p.u.)	Vmax (p.u.)	Vmin (p.u.)
1	3	0	0	1.06	0	1.1	0.95
2	2	21.7	12.7	1.045	-4.98	1.1	0.95
3	2	94.2	19	1.01	-12.72	1.1	0.95
4	1	47.8	-3.9	1.019	-10.33	1.1	0.95
5	1	7.6	1.6	1.02	-8.78	1.1	0.95
6	1	11.2	7.5	1.07	-14.22	1.1	0.95

7	1	0	0	1.062	-13.37	1.1	0.95
8	1	0	0	1.09	-13.36	1.1	0.95
9	1	29.5	16.6	1.056	-14.94	1.1	0.95
10	1	9	5.8	1.051	-15.1	1.1	0.95
11	1	3.5	1.8	1.057	-14.79	1.1	0.95
12	1	6.1	1.6	1.055	-15.07	1.1	0.95
13	1	13.5	5.8	1.05	-15.16	1.1	0.95
14	1	14.9	5	1.036	-16.04	1.1	0.95

V: Generator Parameters for IEEE 14-Bus Test System

Bus No	**Pg (MW)**	**Qg (MVAr)**	**Qmax (MVAr)**	**Qmin (MVAr)**	**Vg (p.u.)**	**Pmax (MW)**	**Pmin (MVAr)**	**X (p.u)**	**H**
1	232.4	-16.9	10	0	1.06	332.4	0	0.3	5.148
2	40	42.4	50	-40	1.045	140	0	0.19	6.54
3	0	23.4	40	0	1.01	100	0	0.185	6.54
6	0	12.2	24	-6	1.07	100	0	0.232	5.06
8	0	17.4	24	-6	1.09	100	0	0.232	5.06

VI: Branch Parameters for IEEE 14-Bus Test System

From Bus	**To Bus**	**R (p.u.)**	**X (p.u.)**	**B (p.u.)**
1	2	0.01938	0.05917	0.0528
1	5	0.05403	0.22304	0.0492
2	3	0.04699	0.19797	0.0438
2	4	0.05811	0.17632	0.034
2	5	0.05695	0.17388	0.0346
3	4	0.06701	0.17103	0.0128
4	5	0.01335	0.04211	0
4	7	0	0.20912	0
4	9	0	0.55618	0
5	6	0	0.25202	0
6	11	0.09498	0.1989	0
6	12	0.12291	0.25581	0
6	13	0.06615	0.13027	0
7	8	0	0.17615	0
7	9	0	0.11001	0
9	10	0.03181	0.0845	0
9	14	0.12711	0.27038	0
10	11	0.08205	0.19207	0
12	13	0.22092	0.19988	0
13	14	0.17093	0.34802	0